Formation of Arrays of Gallium Nitride Nanorods within Mesoporous Silica SBA-15

Cheng-Tzu Yang and Michael H. Huang*

Department of Chemistry, National Tsing Hua University, Hsinchu 30013, Taiwan

Received: April 29, 2005; In Final Form: June 28, 2005

We report the first formation of arrays of GaN nanorods inside the nanoscale channels of mesoporous silica SBA-15. $GaCl_3$ dissolved in toluene was incorporated into the methyl group-functionalized SBA-15 powder. The pore surfaces functionalized with methyl groups should facilitate the impregnation with $GaCl_3$. Formation of GaN nanorod arrays within SBA-15 was carried out by heating the powder to 700 °C for 3 h under nitrogen atmosphere, followed by ammonolysis at 900 °C for 5 h. ϵ-Ga_2O_3, an unusual phase for Ga_2O_3, formed after the first thermal process and was converted into wurtzite GaN during ammonolysis. The final products have been characterized by FT-IR spectra, powder XRD patterns, TEM images and SAED patterns, EDS analysis, and nitrogen adsorption−desorption isotherm measurements to confirm the presence of GaN nanostructures. The nanorods are 6−7.5 nm in diameter, and can be a few hundreds of a nanometer in length to exhibit nanowire structure. Free-standing GaN nanorod arrays were revealed upon removal of the silica framework with HF solution. Optical characterization of the isolated GaN nanorod arrays shows a strong and sharp near band-edge emission at 375 nm, and two phonon-assisted donor−acceptor peaks at 395 and 415 nm. A broad but weak emission in the region of 335−360 nm due to the quantum confinement effect of short nanorods was observed.

Introduction

Formation of metal and semiconductor nanoparticles and nanowires within the nanoscale channels of mesoporous silica materials has been an active area of research interest in recent years. The pore diameters of the channels limit the sizes of the embedded nanoparticles and the diameters of the incorporated nanowires. This template-assisted growth approach enables the formation of nanoparticles and nanowires with interesting size-dependent physical properties, as has been demonstrated for $Zn_{1-x}Mn_xS$ nanowires formed within mesoporous silica MCM-41 and SBA-15.[1] Most of the studies involve the formation of metal nanoparticles and nanowires, such as Au,[2−8] Ag,[2,9] Pt,[2,5−8,10−12] Pd,[13−17] Ru,[18] and Ti,[19] within the nanoscale channels of mesoporous silica powder and thin films. Several studies have explored the preparation of binary semiconductor nanoparticles such as CdS and CdSe inside mesoporous silica powder and films.[20−23] Formation of nanowires of β-MnO_2 in the pores of SBA-15 has also been studied.[24] Metal nanoparticles confined within the channels of mesoporous silica materials may find applications in heterogeneous catalysis, while incorporation of semiconductor nanocrystals may reveal unique optical properties.

With the exceptions of the synthesis of quantum-confined GaN nanoparticles in MCM-41 powder and TiN nanoparticles in SBA-15 powder, the formation of nitride nanostructures within mesoporous silica has not been reported.[25,26] Formation of GaN nanorods and nanowires within mesoporous silica should be very attractive. GaN is an important III−V semiconductor with a direct band gap of 3.39 eV. GaN nanowires have been shown to exhibit UV lasing and field emission properties.[27,28] Fabrication of nanoscale ultraviolet light-emitting diodes with GaN nanorods has also been demonstrated.[29] These GaN nanowires are typically prepared via the chemical vapor deposition method. GaN nanoparticles can be synthesized via solution phase approach through the reaction between $GaCl_3$ and NaN_3.[30] The resulting particles have diameters of several tens of nanometers. Solvothermal synthesis of GaN nanoparticles with 2−4 nm particle size has been carried out with GaN precursors dimeric amidogallium $Ga_2[N(CH_3)_2]_6$ and Ga Cupferron derivative $Ga(C_6H_5N_2O_2)_3$.[31,32] The successful preparation of these ultra-small GaN nanoparticles has enabled the observation of quantum-confined optical properties. These GaN quantum dots are spherical in shape; formation of rodlike GaN nanostructures with diameters of a few nanometers still has not been demonstrated. Mesoporous silica SBA-15 with larger pore channels than those of MCM-41 materials may be a suitable candidate for the template synthesis of elongated GaN nanostructures. Here we describe the first growth of arrays of GaN nanorods within the channels of SBA-15 powder. $GaCl_3$ was used as the precursor in the present study and was dissolved in toluene for loading into SBA-15. Pyrolysis of the precursor in the methyl group-modified channels of SBA-15 under flowing nitrogen and then ammonia resulted in the formation of GaN nanorod arrays. The presence and distribution of GaN nanorod arrays within SBA-15 were confirmed by several characterization techniques. Photoluminescence spectra of the isolated GaN nanorod arrays were taken to examine the optical properties of these GaN nanostructures.

Experimental Section

Mesoporous silica SBA-15 was synthesized following our previously described procedure with slight modification.[26] First, 4 g of triblock copolymer Pluronic P123 surfactant (BASF) was added to a solution of 30 g of deionized water and 120 g of 2 M HCl at 40 °C with stirring until the copolymer has completely dissolved. Then 8.5 g of tetraethyl orthosilicate (TEOS) was added, and the resulting mixture was heated at 40 °C for 6 h.

* To whom correspondence should be addressed. E-mail: hyhuang@mx.nthu.edu.tw.

10.1021/jp052228k CCC: $30.25
Published on Web 08/31/2005

The mixture was transferred to a sealed container and was kept at 100 °C in an oven for 20 h. The resulting white precipitate was filtered and dried at 100 °C overnight. Finally, the template was removed by calcination at 550 °C for 5 h to obtain fine mesoporous SBA-15 powder.

The hydrophilic nature of the pore channels of SBA-15 due to the presence of silanol groups (Si−OH) was modified with methyl groups to make the pore surfaces more hydrophobic. The precursor $GaCl_3$ is soluble in dry toluene and a more hydrophobic intrachannel surface may facilitate the impregnation with $GaCl_3$ in the mesoporous channels. Prior to surface modification, the calcined SBA-15 was refluxed in deionized water for 1 h and heated in a vacuum at 150 °C to remove water. Then 0.5 g of the rehydrated SBA-15 was suspended in 60 mL of toluene and 40 mL of methyltrimethoxysilane (MTMS, prepared with 50 wt % of ethanol). The mixture was stirred at room temperature for 24 h. After refluxing the mixture at 80 °C for 6 h, the functionalized SBA-15 (Me-SBA-15) was washed with toluene and ethanol and dried in air.

The final step of the process is the impregnation with $GaCl_3$ and then formation of GaN nanostructures in Me-SBA-15. First, 0.1 g of the Me-SBA-15 powder was mixed with 1 g of $GaCl_3$ in a flask under nitrogen atmosphere, followed by injection of dry toluene into the flask as a solvent. The mixture was stirred at room temperature under nitrogen flow for 24 h. The product was filtered in the air and rinsed with toluene to remove excess precursor from the external surface of Me-SBA-15. The sample was then dried at 150 °C in a vacuum for 2 h. After that, the powder was placed in a ceramic boat, and the boat was inserted into the center of a tube furnace. The furnace quartz tube used has a 1-in. diameter. The quartz tube was purged with nitrogen for 1 h before raising the furnace temperature to 700 °C for 3 h under a constant flow of nitrogen (100 sccm). Then the furnace was cooled to room temperature. To form GaN nanostructures, the quartz tube was subsequently purged with ammonia for 1 h and the furnace temperature was increased to 900 °C and kept for 5 h under a constant flow of ammonia (100 sccm). The GaN-incorporated SBA-15 can be collected after cooling the furnace to room temperature. To obtain free-standing GaN nanorod arrays, the silica framework was removed by adding a drop of 48 wt % HF solution to the GaN-incorporated SBA-15 powder. The HF-powder solution became clear, indicating the dissolution of the silicate matrix. Part of the solution was transferred to a TEM grid and dried for analysis.

Results and Discussion

The silanol groups (Si−OH) on the channel surfaces of SBA-15 were modified with methyl groups to facilitate the impregnation with toluene-dissolved $GaCl_3$ in the mesoporous channels. The methyl group-functionalized SBA-15, or Me-SBA-15, was investigated by Fourier transform infrared spectroscopy (FT-IR) using a Perkin-Elmer Spectrum RX I spectrometer. Figure 1 shows the FT-IR spectrum of calcined and methyl group-functionalized SBA-15 powder. The IR bands were assigned according to two IR spectroscopy reference books and a paper.[33−35] The difference in the baseline percent transmittance of the two samples is due to slightly different amounts of SBA-15 samples used in the FT-IR measurements. Several new bands appear in the Me-SBA-15 sample. The bands at 2850 and 2983 cm^{-1} correspond to the symmetric and asymmetric C−H stretches of $-CH_3$, respectively. The band at 1276 cm^{-1} corresponds to the symmetric CH_3 deformation vibrations of $Si-CH_3$. The presence of these IR bands indicates that the channel surface of calcined SBA-15 powder has been modified

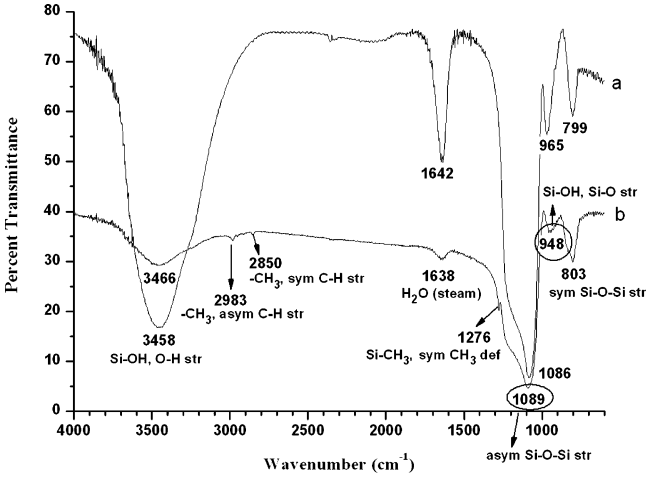

Figure 1. FT-IR spectra of (a) calcined SBA-15 powder and (b) methyl group-functionalized SBA-15 powder. The types of vibrations involved are also indicated.

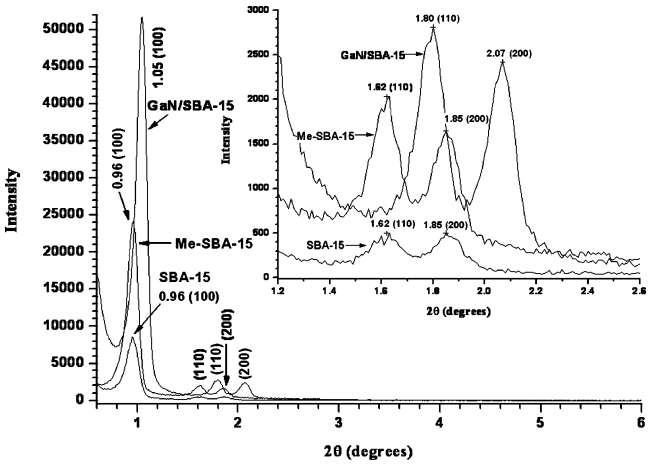

Figure 2. Small-angle XRD patterns of calcined SBA-15, methyl group-functionalized SBA-15, and GaN-incorporated SBA-15. The inset shows the enlarged XRD patterns of the same samples.

with methyl groups. The large reduction in the absorbance of the O−H stretch band in the Me-SBA-15 sample also suggests the replacement of hydroxyl groups with methyl groups.

Retention of high-quality mesoporous SBA-15 after the postsynthesis treatments and the formation of GaN nanostructures can be confirmed by powder X-ray diffraction (XRD) patterns. XRD patterns were collected using a Shimadzu XRD-7000 diffractometer with Cu Kα radiation at $\lambda = 1.5418$ Å. Figure 2 shows the XRD patterns of calcined SBA-15, Me-SBA-15, and GaN-incorporated SBA-15 samples. All three samples show strong (100), (110), and (200) diffraction peaks, indicating the presence and maintenance of long-range mesoporous structure in the GaN-incorporated SBA-15 sample. The (100) peak of the calcined SBA-15 sample is at 0.96° 2θ corresponding to a d spacing of 92.0 Å. After methyl group functionalization, the positions of all diffraction peaks are unchanged. A slight shrinkage in the mesoporous framework is detected for the GaN-incorporated SBA-15 sample. The (100) peak is shifted to 1.05° 2θ corresponding to a d spacing of 84.1 Å, possibly due to a higher degree of silicate condensation after the heat treatment. Figure 3a shows the high-angle powder XRD pattern of GaN nanostructure-incorporated SBA-15 after ammonolysis was performed at 900 °C for 5 h. The diffraction pattern matches well with that of hexagonal wurtzite GaN, confirming the successful formation of GaN nanostructures. The diffraction peaks are weak and relatively broad due to their

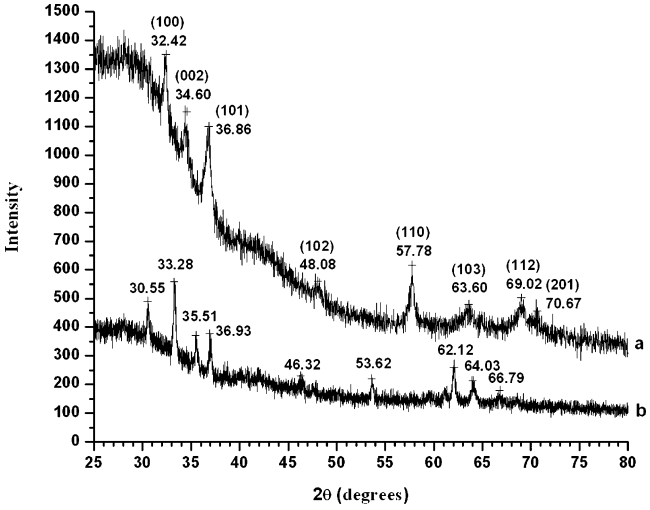

Figure 3. (a) XRD pattern of GaN-incorporated SBA-15 after ammonolysis at 900 °C for 5 h. The broad signal at 25−30° 2θ comes from the silica framework. (b) XRD pattern of the $GaCl_3$-loaded Me-SBA-15 powder recorded after 3 h of heat treatment at 700 °C under a nitrogen flow. The peaks are attributed to the formation of ϵ-Ga_2O_3.

nanoscale dimensions. However, the estimated particle size calculated using the Sherrer equation is about 9−10 nm, larger than the pore diameter. This is not due to the presence of particles outside the SBA-15 powder, as such particles were not observed in the TEM images. Maybe the rodlike GaN nanostructures produce a larger crystalline domain size. Figure 3b gives the XRD pattern of the Me-SBA-15 powder after impregnation with $GaCl_3$ and heat treatment at 700 °C under a nitrogen flow. The diffraction pattern matches well with that of ϵ-Ga_2O_3 (JCPDS 06-0509), which is a rarely observed phase for Ga_2O_3 and indexing of the peaks is not available. The more typical crystal phase for Ga_2O_3 is monoclinic β-Ga_2O_3. Therefore during the GaN nanostructure formation process, ϵ-Ga_2O_3 is formed first and is then completely converted into GaN. The formation of GaN through high-temperature ammonolysis of Ga_2O_3 has been reported with the proposed reaction $Ga_2O_3 + 2NH_3 \rightarrow 2GaN + 3H_2O$.[36,37]

Direct evidence of the formation of GaN nanostructure-incorporated SBA-15 powder was obtained by transmission electron microscopy (TEM) images. A JEOL JEM-2010 transmission electron microscope operated at 200 kV and equipped with an energy-dispersive X-ray spectrometer (EDS) was used for the TEM characterization of the sample. Figure 4 shows the TEM image of GaN-incorporated SBA-15. It reveals the presence of arrays of elongate GaN nanostructures confined within the nanoscale channels of SBA-15 powder. The growth of these GaN nanostructures also follows the curvature of the channels. These nanostructures show an estimated diameter of ~6.5 nm, consistent with the pore channel diameter measured from the nitrogen adsorption experiment (data shown later). The selected-area electron diffraction (SAED) pattern taken over the more GaN nanostructure-concentrated area of the sample gives a ring pattern that resembles the electron diffraction pattern for polycrystalline GaN (SAED pattern of the free-standing GaN and indexing of the rings are shown later). Figure 5 gives a high-resolution TEM image of some short GaN nanorods within SBA-15. The diameters of the nanorods are close to those of the pore channels. Clear lattice fringes can be seen with a measured spacing between adjacent lattice planes of ~2.76 Å, and are attributed to the (100) family of planes of GaN.

Figure 4. TEM image of GaN-incorporated SBA-15 after ammonolysis at 900 °C for 5 h. Arrays of GaN nanostructures (the dark streaks and spots) line up along the curved channels of SBA-15. The inset shows the corresponding selected-area electron diffraction pattern of the sample.

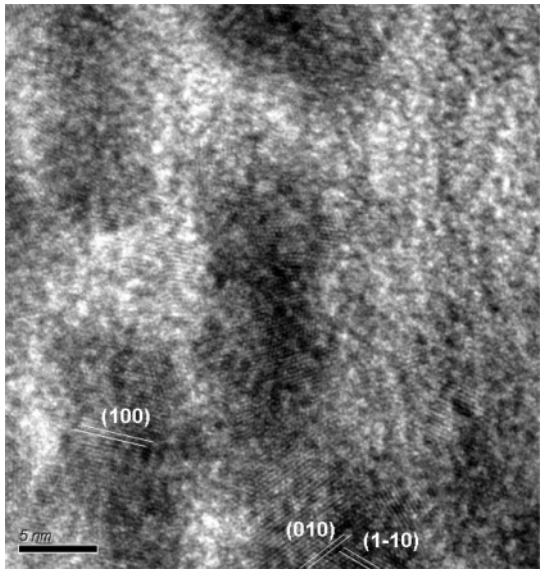

Figure 5. High-resolution TEM image of short GaN nanorods confined in the channels of SBA-15. Lattice fringes correspond to the (100) lattice planes of GaN.

Solid evidence of the formation of GaN nanostructures can be obtained by the removal of the silica framework with HF solution to reveal the isolated GaN nanostructures. Figure 6a displays the TEM image of the free-standing GaN nanostructures after silicate matrix removal. Dense arrays of GaN nanorods are present. These nanorods appear to link together to form nanowire structure a few hundreds of nanometer in length. The adjacent nanorods or nanowires are aligned side-by-side. It may be that the relative positions and orientations of adjacent nanorods are largely preserved after the silicate matrix removal to give this aligned nanorod superstructure. Close examination of the TEM image (Figure 6b) shows that the nanowire structure is formed through the linkage of individual GaN nanorods

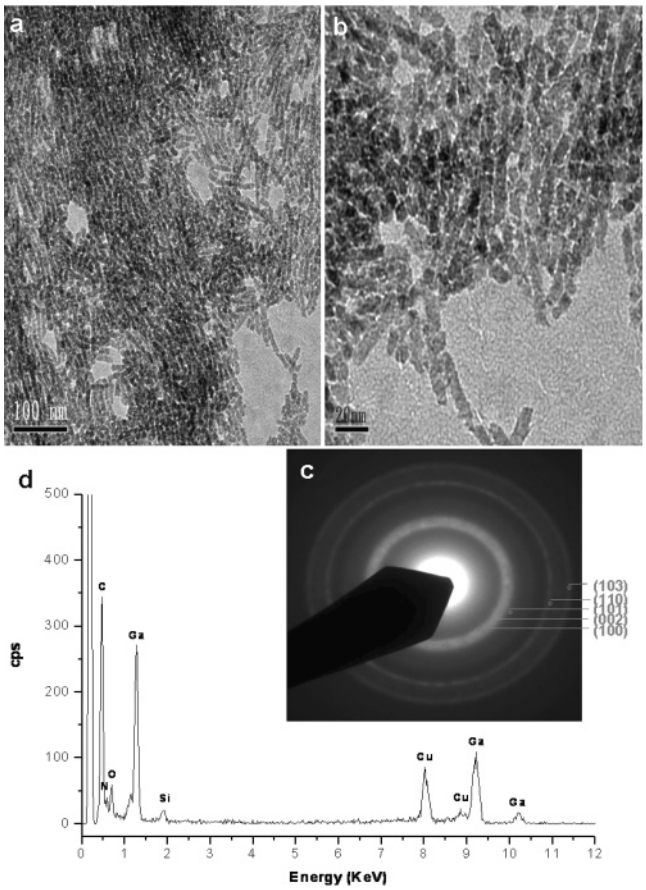

Figure 6. (a) TEM image of the free-standing GaN nanorod arrays. (b) High-magnification TEM image of a portion of the image in panel a. (c) Selected-area electron diffraction pattern of the GaN nanorod arrays in panel b. (d) Energy-dispersive X-ray analysis of the GaN nanorod arrays in panel b.

several tens of nanometers in length. The diameters of these nanorods range between 6 and 7.5 nm, in agreement with the measured diameters of the pore channels. SAED pattern of the isolated GaN nanorod arrays (Figure 6c) gives a ring pattern that can be indexed to the (100), (002), (101), (110), and (103) planes of hexagonal GaN, confirming the composition of the nanorods as GaN. EDS analysis of the GaN nanorod array structure (Figure 6d) shows strong Ga signals and the presence of nitrogen, further indicating that these nanostructures are composed of gallium and nitrogen. The Si and O signals presumably come from the dissolved silicate species, whereas the Cu and C signals are from the carbon-coated copper grid.

The degree of GaN nanorod loading within SBA-15 was investigated using nitrogen adsorption−desorption isotherm measurements. These measurements were performed at 77 K using a Micromeritics ASAP 2010 system. Figure 7a shows the nitrogen adsorption−desorption isotherm results for the calcined SBA-15, Me-SBA-15, and GaN-incorporated SBA-15 samples. The pore diameter distribution of these samples is plotted in Figure 7b. Summary of the BET surface areas, total pore volumes, and pore diameters of these samples is given in Table 1. Reductions in the BET surface area and total pore volume were obtained for the Me-SBA-15. The total pore volume decreases from 0.92 $cm^3\ g^{-1}$ for the calcined SBA-15 to 0.80 $cm^3\ g^{-1}$ for the Me-SBA-15. These results are attributed to the intrachannel surface functionalization with a layer of methyl groups. Significant decrease in the total pore volume to 0.53 $cm^3\ g^{-1}$ was measured for the GaN-incorporated SBA-15 sample. This large decrease in the total pore volume indicates

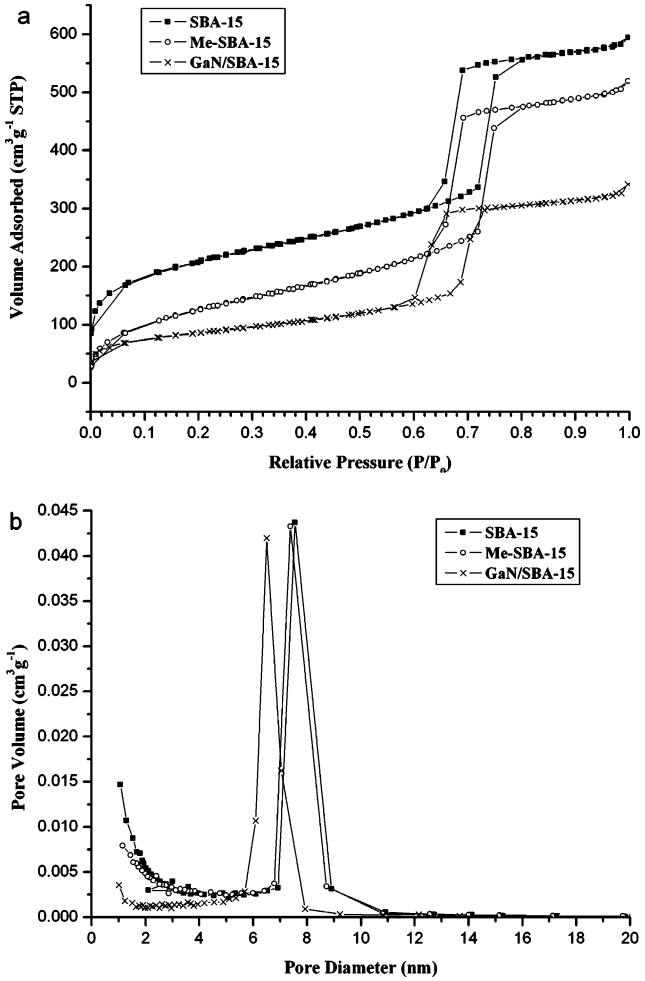

Figure 7. (a) Nitrogen adsorption−desorption isotherms of calcined SBA-15 (■), methyl group-functionalized SBA-15 (○), and GaN-incorporated SBA-15 (×). (b) Pore diameter distribution of the samples calculated from the desorption branch of the isotherms using the BJH algorithm.

TABLE 1: Nitrogen Adsorption−Desorption Isotherm Data[a] and the *d*-Spacings of the (100) X-ray Diffraction Peak for the Three SBA-15 Samples

	nitrogen adsorption isotherms			XRD patterns
sample	$S_{BET}/m^2\ g^{-1}$	$V_t/cm^3\ g^{-1}$	D_{BJH}/nm	$d_{(100)}$/nm
SBA-15	735	0.92	7.6	9.2
Me-SBA-15	483	0.80	7.4	9.2
GaN/SBA-15	307	0.53	6.5	8.4

[a] S_{BET}, BET specific surface area; V_t, total pore volume; D_{BJH}, pore diameter calculated using the BJH method.

that there is a significant degree of pore filling with the GaN nanostructures. The weight percentage loading of GaN was calculated to be about 54%, following the method described previously.[26] The pore diameter for the Me-SBA-15 is 7.4 nm, which is essentially the same as that for the calcined SBA-15. However, a substantial decrease in the pore diameter for the GaN-incorporated SBA-15 was observed (that is, to 6.5 nm). The high-temperature ammonolysis at 900 °C for 5 h may further increase the degree of silicate condensation and lead to a shrinkage in the pore diameter. The wall thicknesses, however, remained relatively unchanged for all the samples at 3 nm, as calculated from the pore diameters and the *d*-spacings of the (100) peak in their XRD patterns.[38] The pore diameter distribution of the GaN-incorporated SBA-15 sample is narrower than the other two samples, which may explain the extremely high

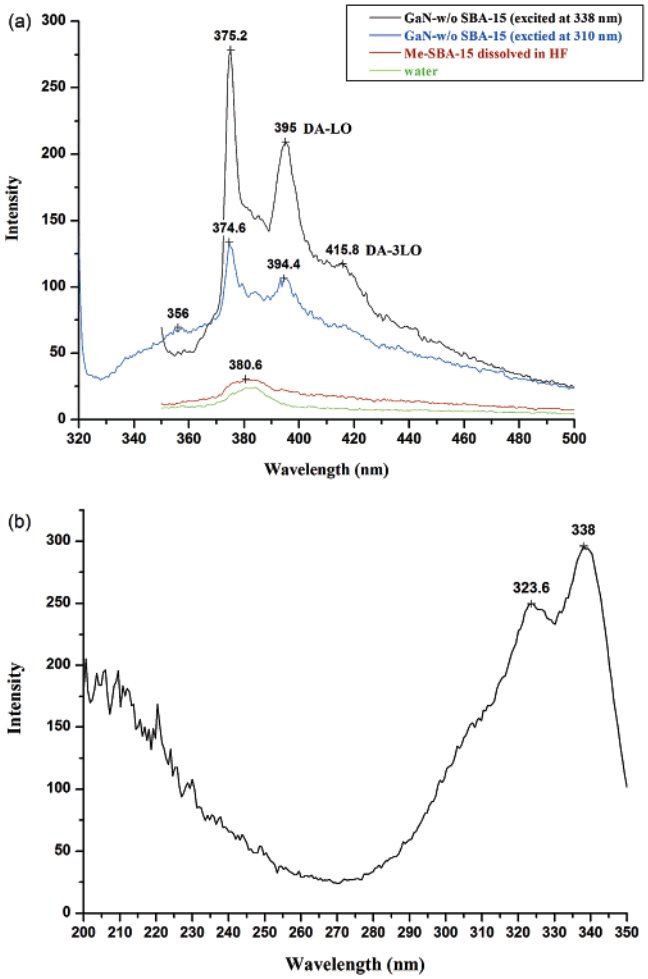

Figure 8. (a) Photoluminescence spectra of the isolated GaN nanorod arrays after the removal of the silica framework (black line), methyl group-functionalized SBA-15 dissolved in HF solution (red line), and pure water (green line) excited at 338 nm. Photoluminescence spectrum of the same sample but excited at 310 nm is also shown here (blue line). (b) Excitation spectrum of the isolated GaN nanorod arrays monitored at 375 nm.

intensity of the (100) peak in its XRD pattern as this sample possesses a better long-range mesostructure after the high-temperature postsynthesis treatments.

Photoluminescence spectra of the GaN nanorod arrays were taken to examine their optical properties. A Hitachi F-4500 fluorescence spectrophotometer was used for the photoluminescence study. Figure 8a shows the photoluminescence spectrum of the isolated GaN nanorod arrays excited at 338 nm. Several emission peaks at 375, 395, and 415 nm can be identified. No other emission peaks were observed beyond 500 nm. Figure 8b is the excitation spectrum of the GaN nanorod arrays monitored at 375 nm. It shows two excitation peaks at 324 and 338 nm. Light emission from the GaN nanorod arrays was found to be sensitive to the excitation wavelength; no emission peaks were observed when the GaN nanorod arrays were excited from 250 to before 310 nm. To assist in the assignment of these peaks, the photoluminescence spectrum of the Me-SBA-15 dissolved in HF solution was taken (Figure 8a). It shows a spectrum identical with that of pure water with a weak emission peak at ~380 nm. Thus all the major identified emission peaks are believed to come from the luminescence of the GaN nanorod arrays, not from the silica framework. The peak at 375 nm is attributed to the near band-edge emission (band gap energy, $E_g = 3.39$ eV).[37] The peaks at 395 and 415 nm are assigned as the longitudinal optical (LO) phonon replica donor−acceptor (DA) and 3-LO phonon replica DA peaks, respectively.[39−41] These emission peaks have also been observed in bulk GaN and commercial GaN, and thus are the typical emission peaks for GaN.[39,42] However, the sharpness of the 375-nm near band-edge emission may be related to the quantum confinement effect and indicates that the discrete energy levels have taken the place of the continuous energy band.[43] GaN nanoparticles 4−5 nm in size have been shown to exhibit an additional emission peak at 315−317 nm.[32,43] To see if this additional emission peak due to the quantum confinement effect may be present, the sample was excited at 310 nm and the spectrum obtained is also shown in Figure 8a. A broad but weak emission band in the region of 335−360 nm was observed. This broad blue-shifted emission is attributed to the quantum-confined emission from some short GaN nanorods with a wide distribution of lengths (Bohr exciton radius for GaN is 11 nm).[44] However, many nanorods may be so long that they do not show this blue-shifted emission, even though these nanorods are only 6−7.5 nm in diameter. It has been shown that as particle size increases or elongates into rodlike structure, the quantum-confined emission peak may rapidly red-shift toward the position of the near band-edge emission (as observed for CdSe nanorods) or disappear.[32,45] The present results suggest that a large fraction of the individual nanorods and the extended nanorod arrays are so long that they mainly show the near band-edge emission at 375 nm.

Conclusion

The formation of arrays of GaN nanorods within the nanoscale channels of SBA-15 has been demonstrated. $GaCl_3$ dissolved in toluene was used as the gallium precursor and introduced into the interior of the methyl group-functionalized SBA-15 powder. Heat treatment at 700 °C under nitrogen flow produced an unusual ϵ-Ga_2O_3 phase. Subsequent ammonolysis at 900 °C resulted in the formation of arrays of GaN nanorods. The nanorods have diameters of 6−7.5 nm and can be a few hundreds of nanometer in length to exhibit nanowire structure. The formation process and the existence of these GaN nanorod arrays have been examined by FT-IR spectra, XRD patterns, TEM images, SAED patterns, EDS spectrum, and nitrogen adsorption−desorption isotherm measurements. Photoluminescence spectra of the isolated GaN nanorod arrays excited at 338 nm show a strong near band-edge emission at 375 nm, and two phonon-assisted donor−acceptor peaks at 395 and 415 nm. The extreme sharpness of the 375-nm peak may be related to the quantum confinement effect. In addition, a broad but weak emission in the region of 335−360 nm was observed when excited at 310 nm. This is attributed to the quantum-confined emission from short nanorods. This work demonstrates the feasibility of forming rodlike GaN nanostructures using the mesoporous silica SBA-15 template. Other binary nitride nanorod structures may be synthesized by using a preparation approach similar to that described in this study, and enable the examination of novel physical properties. The unexpected formation of ϵ-Ga_2O_3 by this template-assisted route deserves further investigation, and research work is in progress.

Acknowledgment. This work was supported by a grant from the National Science Council of Taiwan (NSC 93-2113-M-007-034). We thank Men-Liang Lin for assistance in the nitrogen physisorption measurements and Yeng-Po Chang for sample preparation for TEM examination of GaN-incorporated SBA-

15. We also thank Prof. Hong-Yi Tang for assistance in the powder XRD pattern measurements.

References and Notes

(1) Brieler, F. J.; Grundmann, P.; Fröba, M.; Chen, L.; Klar, P. J.; Heimbrodt, W.; von Nidda, H.-A. K.; Kurz, T.; Loidl, A. *J. Am. Chem. Soc.* **2004**, *126*, 797.

(2) Han, Y.-J.; Kim, J. M.; Stucky, G. D. *Chem. Mater.* **2000**, *12*, 2068.

(3) Kónya, Z.; Puntes, V. F.; Kiricsi, I.; Zhu, J.; Ager, J. W., III; Ko, M. K.; Frei, H.; Alivisatos, P.; Somorjai, G. A. *Chem. Mater.* **2003**, *15*, 1242.

(4) Yan, W.; Chen, B.; Mahurin, S. M.; Hagaman, E. W.; Dai, S.; Overbury, S. H. *J. Phys. Chem. B* **2004**, *108*, 2793.

(5) Yang, C.-M.; Liu, P.-H.; Ho, Y.-F.; Chiu, C.-Y.; Chao, K.-J. *Chem. Mater.* **2003**, *15*, 275.

(6) Yang, C.-M.; Sheu, H.-S.; Chao, K.-J. *Adv. Funct. Mater.* **2002**, *12*, 143.

(7) Fukuoka, A.; Araki, H.; Sakamoto, Y.; Sugimoto, N.; Tsukada, H.; Kumai, Y.; Akimoto, Y.; Ichikawa, M. *Nano Lett.* **2002**, *2*, 793.

(8) Kónya, Z.; Puntes, V. F.; Kiricsi, I.; Zhu, J.; Alivisatos, A. P.; Somorjai, G. A. *Nano Lett.* **2002**, *2*, 907.

(9) Huang, M. H.; Choudrey, A.; Yang, P. *Chem. Commun.* **2000**, 1063.

(10) Shin, H. J.; Ryoo, R.; Liu, Z.; Terasaki, O. *J. Am. Chem. Soc.* **2001**, *123*, 1246.

(11) Liu, Z.; Sakamoto, Y.; Ohsuna, T.; Hiraga, K.; Terasaki, O.; Ko, C. H.; Shin, H. J.; Ryoo, R. *Angew. Chem., Int. Ed.* **2000**, *39*, 3107.

(12) Shin, H. J.; Ko, C. H.; Ryoo, R. *J. Mater. Chem.* **2001**, *11*, 260.

(13) Wang, D.; Zhou, W. L.; McCaughy, B. F.; Hampsey, J. E.; Ji, X.; Jiang, Y.-B.; Xu, H.; Tang, J.; Schmehl, R. H.; O'Connor, C.; Brinker, C. J.; Lu, Y. *Adv. Mater.* **2003**, *15*, 130.

(14) Lee, K.-B.; Lee, S.-M.; Cheon, J. *Adv. Mater.* **2001**, *13*, 517.

(15) Zhang, Z.; Dai, S.; Blom, D. A.; Shen, J. *Chem. Mater.* **2002**, *14*, 965.

(16) Yuranov, I.; Kiwi-Minsker, L.; Buffat, P.; Renken, A. *Chem. Mater.* **2004**, *16*, 760.

(17) Li, L.; Shi, J.-L.; Zhang, L.-X.; Xiong, L.-M.; Yang, J.-N. *Adv. Mater.* **2004**, *16*, 1079.

(18) Li, H.; Wang, R.; Hong, Q.; Chen, L.; Zhong, Z.; Koltypin, Y.; Calderon-Moreno, J.; Gedanken, A. *Langmuir* **2004**, *20*, 8352.

(19) Luan, Z.; Maes, E. M.; van der Heide, P. A. W.; Zhao, D.; Czernuszewicz, R. S.; Kevan, L. *Chem. Mater.* **1999**, *11*, 3680.

(20) Besson, S.; Gacoin, T.; Ricolleau, C.; Jacquiod, C.; Boilot, J.-P. *Nano Lett.* **2002**, *2*, 409.

(21) Xu, W.; Liao, Y.; Akins, D. L. *J. Phys. Chem. B* **2002**, *106*, 11127.

(22) Zhang, Z.; Dai, S.; Fan, X.; Blom, D. A.; Pennycook, S. J.; Wei, Y. *J. Phys. Chem. B* **2001**, *105*, 6755.

(23) Parala, H.; Winkler, H.; Kolbe, M.; Wohlfart, A.; Fischer, R. A.; Schmechel, R.; von Seggern, H. *Adv. Mater.* **2000**, *12*, 1050.

(24) Imperor-Clerc, M.; Bazin, D.; Appay, M.-D.; Beaunier, P.; Davidson, A. *Chem. Mater.* **2004**, *16*, 1813.

(25) Winkler, H.; Birkner, A.; Hagen, V.; Wolf, I.; Schmechel, R.; von Seggern, H.; Fischer, R. A. *Adv. Mater.* **1999**, *11*, 1444.

(26) Hsueh, H.-S.; Yang, C.-T.; Zink, J. I.; Huang, M. H. *J. Phys. Chem. B* **2005**, *109*, 4404.

(27) Johnson, J. C.; Choi, H.-J.; Knutsen, K. P.; Schaller, R. D.; Yang, P.; Saykally, R. J. *Nat. Mater.* **2002**, *1*, 101.

(28) Chen, C.-C.; Yeh, C.-C.; Chen, C.-H.; Yu, M.-Y.; Liu, H.-L.; Wu, J.-J.; Chen, K.-H.; Chen, L.-C.; Peng, J.-Y.; Chen, Y.-F. *J. Am. Chem. Soc.* **2001**, *123*, 2791.

(29) Kim, H.-M.; Kang, T. W.; Chung, K. S. *Adv. Mater.* **2003**, *15*, 567.

(30) (a) Wang, J.; Grocholl, L.; Gillan, E. G. *Nano Lett.* **2002**, *2*, 899. (b) Grocholl, L.; Wang, J.; Gillian, E. G. *Chem. Mater.* **2001**, *13*, 4290.

(31) Mićić, O. I.; Ahrenkiel, S. P.; Bertram, D.; Nozik, A. J. *Appl. Phys. Lett.* **1999**, *75*, 478.

(32) Sardar, K.; Rao, C. N. R. *Adv. Mater.* **2004**, *16*, 425.

(33) Socrates, G. *Infrared Characteristic Group Frequencies*; John Wiley & Sons: Bath, UK, 1980.

(34) Günzler, H.; Gremlich, H.-U. *IR Spectroscopy*; Wiley-VCH: Weinheim, Germany, 2002.

(35) Gu, G.; Ong, P. P.; Chu, C. *J. Phys. Chem. Solids* **1999**, *60*, 943.

(36) Schwenzer, B.; Hu, J.; Seshadri, R.; Keller, S.; DenBaars, S. P.; Mishra, U. K. *Chem. Mater.* **2004**, *16*, 5088.

(37) Sun, X.; Li, Y. *Angew. Chem., Int. Ed.* **2004**, *116*, 3915.

(38) Zhao, D.; Feng, J.; Huo, Q.; Melosh, N.; Fredrickson, G. H.; Chmelka, B. F.; Stucky, G. D. *Science* **1998**, *279*, 548.

(39) Strite, S.; Morkoç, H. *J. Vac. Sci. Technol. B* **1992**, *10*, 1237.

(40) Dingle, R.; Sell, D. D.; Stokowski, S. E.; Ilegems, M. *Phys. Rev. B* **1971**, *4*, 1211.

(41) Jian, J. K.; Chen, X. L.; Tu, Q. Y.; Xu, Y. P.; Dai, L.; Zhao, M. *J. Phys. Chem. B* **2004**, *108*, 12024.

(42) Grocholl, L.; Wang, J.; Gillan, E. G. *Chem. Mater.* **2001**, *13*, 4290.

(43) Gonsalves, K. E.; Rangarajan, S. P.; Carlson, G.; Kumar, J.; Yang, K.; Benaissa, M.; José-Yacaman, M. *Appl. Phys. Lett.* **1997**, *71*, 2175.

(44) Xie, Y.; Qian, Y.; Wang, W.; Zhang, S.; Zhang, Y. *Science* **1996**, *222*, 1926.

(45) Li, L.-S.; Hu, J.; Yang, W.; Alivisatos, A. P. *Nano Lett.* **2001**, *1*, 349.